THE JOURNAL OF PHYSICAL CHEMISTRY B

Article

Influence of Preformed Asp23#Lys28 Salt Bridge on the Conformational Fluctuations of Monomers and Dimers of A# Peptides with Implications for Rates of Fibril Formation

Govardhan Reddy, John E. Straub, and D. Thirumalai

J. Phys. Chem. B, **2009**, 113 (4), 1162-1172 • DOI: 10.1021/jp808914c • Publication Date (Web): 06 January 2009

Influence of Preformed Asp23−Lys28 Salt Bridge on the Conformational Fluctuations of Monomers and Dimers of Aβ Peptides with Implications for Rates of Fibril Formation

Govardhan Reddy

Biophysics Program, Institute for Physical Sciences and Technology University of Maryland, College Park, Maryland 20742

John E. Straub

Department of Chemistry, Boston University, Boston, Massachusetts 02215

D. Thirumalai*

Biophysics Program, Institute for Physical Sciences and Technology and Department of Chemistry and Biochemistry, University of Maryland, College Park, Maryland 20742

Received: October 8, 2008

Recent experiments have shown that the congener Aβ_{1-40}[D23−K28], in which the side chains of charged residues Asp23 and Lys28 are linked by a lactam bridge, forms amyloid fibrils that are structurally similar to the wild type (WT) Aβ peptide, but at a rate that is nearly 1000 times faster. We used all atom molecular dynamics simulations in explicit water, and two force fields, of the WT dimer, a monomer with the lactam bridge (Aβ_{10-35}-lactam[D23−K28]), and the monomer and dimers with harmonically constrained D23−K28 salt bridge (Aβ_{10-35}[D23−K28]) to understand the origin of the enhanced fibril rate formation. The simulations show that the assembly competent fibril-like monomer (N*) structure, which is present among the conformations sampled by the *isolated monomer*, with strand conformations in the residues spanning the N and C termini and a bend involving residues D^{23} $VGSNKG^{29}$, are populated to a much greater extent in Aβ_{10-35}[D23−K28] and Aβ_{10-35}-lactam[D23−K28] than in the WT, which has negligible probability of forming N*. The salt bridge in N* of Aβ_{10-35}[D23−K28], whose topology is similar to that found in the fibril, is hydrated. The reduction in the free energy barrier to fibril formation in Aβ_{10-35}[D23−K28] and in Aβ_{10-35}-lactam[D23−K28], compared to the WT, arises largely due to entropic restriction which enables the bend formation. A decrease in the entropy of the unfolded state and the lesser penalty for conformational rearrangement including the formation of the salt bridge in Aβ peptides with D23−K28 constraint results in a reduction in the kinetic barrier in the Aβ_{1-40}-lactam[D23−K28] congener compared to the WT. The decrease in the barrier, which is related to the free energy cost of forming a bend, is estimated to be in the range $(4-7)k_BT$. Although a number of factors determine the growth of fibrils, the decrease in the free energy barrier, relative to the WT, to N* formation is a major factor in the rate enhancement in the fibril formation of Aβ_{1-40}[D23−K28] congener. Qualitatively similar results were obtained using simulations of Aβ_{9-40} peptides and various constructs related to the Aβ_{10-35} systems that were probed using OPLS and CHARMM force fields. We hypothesize that mutations or other constraints that preferentially enhance the population of the N* species would speed up aggregation rates. Conversely, ligands that lock it in the fibril-like N* structure would prevent amyloid formation.

Introduction

Aggregation of Aβ peptides,[1,2] which are products of proteolytic cleavage of the amyloid-β precursor protein, is linked to the Alzheimers disease.[3] Besides the amyloid plaques, whose major protein component is the Aβ peptide, it has been suggested that soluble oligomers can also be neurotoxic.[4−6] These findings make it important to describe, at the molecular level, the cascade of events that drive the largely unstructured monomer to the ordered amyloid fibril formation. It is generally thought that the isolated Aβ monomer is a fluctuating random coil at neutral pH. Segments of the Aβ peptide are structured, and the large number of heterogeneous conformations can be clustered into several distinct basins.[7] The structures among the basins can interconvert on a broad range of time scales. The structural plasticity associated with the Aβ monomer finds considerable support in several molecular dynamics simulations[7−11] and a few NMR experiments.[12] In contrast, the monomers are ordered in the Aβ amyloid fibril. The Tycko model[13,14] (TM) of the amyloid fibril, which was constructed using a number of solid state NMR derived constraints, shows that roughly the first 10 residues are disordered. The ordered monomer has two β strands that run from residues 10−22 and 30−40 and are connected by a bend comprising of residues 23−29(DVGSNKG). The strands are arranged in a parallel manner so as to maximize the number of hydrophobic contacts and are further stabilized by the D23−K28 salt bridge. Such an arrangement is in accord with the generic principle of amyloid self-assembly (PASA) which is formulated by using a combination of experimental and computational studies.[14−25] According to PASA, stable higher structures (oligomers, protofilaments,

* Corresponding author. E-mail: thirum@umd.edu.

10.1021/jp808914c CCC: $40.75
Published on Web 01/06/2009

and fibrils) are those that maximize the number of intra- and inter-peptide interactions as well as the salt bridges.

It follows from PASA, which emphasizes side-chain packing in the fibrils, that favorable electrostatic interactions must play a role in the early structural organization of soluble Aβ oligomers (dimers, trimers, etc.) that eventually form amyloid fibrils. Indeed, a comparison of the structures of the monomer in isolation and in the fibril shows that the formation of the D23−K28 salt bridge ensures that the unpaired charges are not buried in the low dielectric interior of the fibril. The monomer structure of Aβ peptides can be organized using a transition disconnectivity graph that represents the sampled conformations as a free energy spectrum.[7,8,26] It is likely that many of the conformations are assembly competent, giving rise to fibrils with somewhat different morphology.[14] The average assembly competent structure (N*) of the conformations, in one of the higher free energy basins in the $A\beta_{10-35}$ monomer energy landscape,[7] is similar to that found in the TM model. We stress that the significance of N* is that it is a state that is already present in the monomer and does not typically require inter-peptide interactions to form. In this sense, the postulate that fibril-like N* exists already in the spectrum of monomer conformations is similar to population shift mechanism that has been proposed in the context of allosteric transitions.[27] Thus, an increase in the population of N*, with the intact D23−K28 salt bridge and a bend, which in the wild type (WT) can occur by fluctuations or denaturation stress, can lead to oligomer formation which can convert to amyloid fibril.

The physical picture that the conformations that are accessible in the monomer are assembly competent[28] raises an important question, namely, given that the spontaneous interaction between D23 and K28 in the isolated monomer is free energetically unfavorable, is it possible that monomers with preformed salt bridges can preferentially populate N*, so that ordered fibrils can form more effectively? In a recent study,[29] Sciarretta et al. showed that the aggregation rate in $A\beta_{1-40}$-lactam[D23−K28], in which the residues D23 and K28 are chemically constrained by a lactam bridge, is nearly 1000 times greater than in the WT. The fibrils of the congener $A\beta_{1-40}$-lactam[D23−K28], which are structurally similar to the WT, form without the usual lag phase. Motivated by the experimental findings and building on earlier studies[7−10] on the energy landscape of WT $A\beta_{10-35}$, we have used molecular dynamics (MD) simulations to examine the changes in the conformational fluctuations in the Aβ peptides with a constrained D23−K28 salt bridge.

Previous studies[7,30,31]show that spontaneous formation of a stable D23−K28 salt bridge in the $A\beta_{10-35}$ monomer is unlikely because the barrier to desolvation of the charged residues is too steep for favorable salt bridge formation. The free energy landscape revealed[7] that the basins with conformations containing the D23−K28 salt bridge are metastable. As a result, they are not significantly populated at ambient conditions. Therefore, understanding the conformations sampled by $A\beta_{10-35}$[D23−K28], where the D23−K28 salt bridge is preformed, might shed light on the increased rate[29] of fibril formation in the Aβ-lactam[D23−K28] peptides. The simulations of $A\beta_{10-35}$[D23−K28] can be used to infer if the increased rate in aggregation is due to the decrease in conformational entropy of the Aβ monomer due to the salt bridge constraint or the decrease in the desolvation penalty—an enthalpic effect. Our results suggest that the enhanced fibril formation rate in the lactam congener is helped by entropic restriction in the monomer with the constrained salt bridge. However, enthalpic effects also contribute to the reduction in the free energy barrier to nucleation and growth of $A\beta_{1-40}$-lactam[D23−K28] fibril relative to the WT. The reduction in the conformational entropy and the increased probability of occupying a state, in which the monomer structure closely resembles the one in the fibril, rationalizes the 1000-fold increase in the rate of fibril formation of $A\beta_{1-40}$-lactam[D23−K28] congener. The robustness of our conclusions is established by performing simulations of a number of systems using two force fields.

Theoretical Methods

Peptides. To gain insights into the role of preformed D23−K28 salt bridge in the aggregation process, we simulated several systems, each constructed from the Aβ peptide. It is suspected[16] that the fibrils of $A\beta_{10-35}$ are structurally similar to the full length peptide, thus making the shorter peptide a good surrogate for the $A\beta_{1-40}$ system. In order to examine the effect of inter-peptide interactions, we simulated the $[A\beta_{10-35}]_2$ dimer. We used two methods to constrain the salt bridge between D23 and K28.

Constraining D23−K28 Using Harmonic Potential. The influence of a stable D23−K28 salt bridge on the free energy landscape of the monomer and the dimers is assessed using simulations that constrain the C_γ atom of residue D23 and N_ζ atom of residue K28 by a harmonic potential, $U(r) = (k/2)(r - r_0)^2$. Here, r is the distance between the C_γ atom of residue D23 and N_ζ atom of residue K28 (Figure 1a), and $r_0 = 3.8$ Å is the corresponding equilibrium distance. The value of r_0 is approximately the distance between the C_γ and N_ζ atoms of the salt bridge in the $A\beta_{1-40}$ fibrils.[29] We used $k = 100.0$ kcal/(mol Å^2). The peptide with the constraint is labeled $A\beta_{10-35}$[D23−K28].

Direct Simulation of the Lactam Construct. In order to establish the generality of the results, we also carried out limited set of simulations for $A\beta_{10-35}$-lactam[D23−K28] where there is a lactam bond between the side chain of Asp23 and Lys28 and $A\beta_{9-40}$ monomers. Just as for $A\beta_{10-35}$, we used molecular dynamics simulations for the $A\beta_{10-35}$-lactam[D23−K28], WT $A\beta_{9-40}$, and $A\beta_{9-40}$[D23−K28] in which the salt bridge is constrained.

The advantage of simulating $A\beta_{10-35}$[D23−K28] over $A\beta_{10-35}$-lactam[D23−K28] is that the harmonic restraint induces similar kinds of fluctuations in the peptide as the lactam construct. In addition, we can assess if the bend formed by the residues 23−28 due to the constraint desolvates the charged salt bridge forming atoms. In the presence of the lactam construct, the salt bridge forming atoms are always desolvated due to the presence of a neutral amide bond between the β-carbon of Asp23 and ϵ-carbon of Lys28. The comparison between the two simulations allows us to more fully explore the free energy landscape of the constrained peptides.

Simulations with Two Force Fields. We performed all atom molecular dynamics simulations in explicit solvent using the NAMD[32] simulation package with PARAM22[33] force field of the CHARMM program and the TIP3P model for water. To check for robustness of results, we also performed a limited set of $A\beta_{10-35}$-lactam[D23−K28] monomer simulations using the all atom OPLS force field.[34] Simulations using the OPLS force field are referred to as $A\beta_{10-35}$-lactam[D23−K28](OPLS).

In the simulations, which were done in a cubic cell with periodic boundary conditions, electrostatic interactions were calculated using the particle mesh Ewald summation.[35] The initial coordinates for the $A\beta_{10-35}$ protein were taken from the NMR structure[12] determined at pH 5.6 (Protein Data Bank ID code 1hz3). We used one of the representative structures (Figure

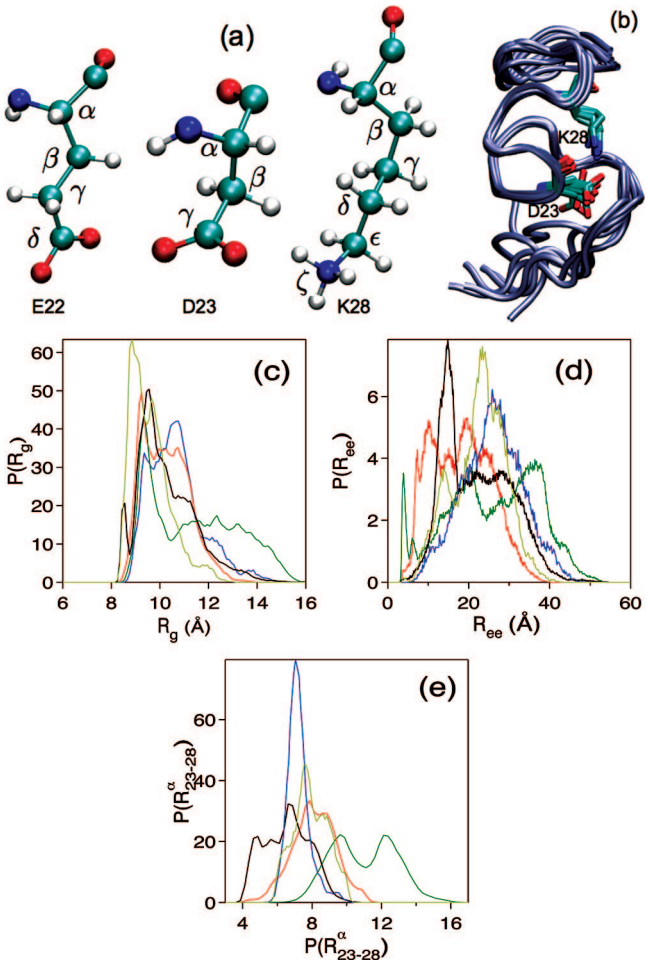

Figure 1. (a) Salt bridge forming residues E22, D23, and K28 in the Aβ peptide. Atoms engaged in salt bridge formation are C_δ atom of residue E22, C_γ atom of residue D23, and N_ζ atom of residue K28. (b) Superposition of a class of NMR structures of Aβ_{10-35} with a salt bridge between D23 and K28 obtained from the Protein Data Bank (1hz3). (c) Probability distribution, $P(R_g)$, of the radius of gyration, $R_g = \{[(1/2N^2)\sum_i\sum_j R_{ij}^2]\}^{1/2}$, where $\vec{R}_{ij}$ is the vector joining the heavy atoms. (d) Probability distribution, $P(R_{ee})$, of the end-to-end distance, R_{ee}, defined as the distance between the C atom of the methyl group in the acetyl cap of the N-terminus and the N atom in the $-NH_2$ group of the amidated C-terminus. (e) Probability distribution, $P(R^{\alpha}_{23-28})$, of the distance between the C_α atoms of residues 23 and 28, R^{α}_{23-28}. In (c), (d), and (e) green, red, black, blue, and yellow lines show the data for WT Aβ_{10-35} dimers, Aβ_{10-35}[D23−K28] dimers, Aβ_{10-35}[D23−K28] monomer, Aβ_{10-35}-lactam[D23−K28] monomer, and Aβ_{10-35}-lactam[D23−K28](OPLS), respectively.

1b) which has a preformed salt bridge between the residues D23 and K28. The monomer from the fibril structure was used as the initial structure in the simulations of Aβ_{9-40} monomers. At pH 5.6, the peptides Aβ_{10-35}, Aβ_{10-35}-lactam[D23−K28], and Aβ_{9-40} are charged, and a chloride ion was added to neutralize the effective charge. The N- and C-terminals of the protein are acetylated and amidated, respectively. The simulations were performed in the NPT ensemble with the temperature $T = 300$ K. Pressure was maintained[36,37] at 1 atm using a Langevin piston. The hydrogen atoms were constrained to the equilibrium positions using the SETTLE[32] algorithm, and a time step of 2 fs is used to integrate the equations of motion.

For the Aβ_{10-35}[D23−K28] monomers, we generated three independent trajectories each 100 ns long. For the wild type dimers, [Aβ_{10-35}]$_2$, and for the D23−K28 salt bridge constrained dimers, [Aβ_{10-35}[D23−-K28]]$_2$, we generated three 70 ns long trajectories. Dimer simulations are performed by placing two monomers at random orientations in a cubic box of size 60 Å. Multiple trajectories (between 3 and 5) of Aβ_{10-35}-lactam-[D23−K28], Aβ_{10-35}-lactam[D23−K28](OPLS), Aβ_{9-40}, and Aβ_{9-40}[D23−K28] are generated, and typically the duration of each trajectory is between 15 and 20 ns. These limited sets of simulations were performed to ensure that there are no qualitative differences in the conclusions based on Aβ_{10-35} and Aβ_{9-40} peptides and in using the harmonic constraint as a surrogate for the lactam bond.

Principal Component Analysis. We used dihedral principal component analysis (DPCA)[38−40] to extract the conformations frequently sampled by the Aβ_{10-35} monomer in the wild type Aβ_{10-35} dimer and Aβ_{10-35}[D23−K28] monomer and dimer simulations. In DPCA, the backbone dihedral angles, α_k, where $\alpha_k \in \{\phi_k, \psi_k\}$, are used with the transformation, $q_k = \cos(\alpha_k)$, $q_{k+1} = \sin(\alpha_k)$, to uniquely define a distance in the space of periodic dihedral angles. The variable k runs form 1 to N, where N is the total number of backbone dihedral angles. The covariance matrix $\sigma_{ij} = \langle(q_i - \langle q_i\rangle)(q_j - \langle q_j\rangle)\rangle$ which probes the correlated internal motions is constructed and diagonalized to extract the eigenvectors V_n, and eigenvalues λ_n, that yield the modes of collective motion and their amplitudes. The free energy surface along the two eigenvectors, V_1 and V_2, which correspond to the first two maximum eigenvalues, λ_1 and λ_2, are given by $\Delta G(V_1, V_2) = -k_B T[\ln P(V_1, V_2) - \ln P_{max}]$. Here $P(V_1, V_2)$ is the probability distribution obtained from a histogram of the MD data. We subtract P_{max}, the maximum of the distribution, to ensure that $\Delta G(V_1, V_2) = 0$ for the lowest free energy minimum; k_B is the Boltzmann constant and T is the temperature.

Results

Aβ_{10-35}[D23−K28] and Aβ_{10-35}-lactam[D23−K28] Monomers Sample Compact Conformations. Constraining the salt bridge with a harmonic force or by using a lactam bond forces the peptides to sample compact conformations which is reflected in the probability distributions, $P(R_g)$, of the radius of gyration (R_g), $P(R_{ee})$ of the end-to-end distance (R_{ee}), and $P(R^{\alpha}_{23-28})$ of the distance, R^{α}_{23-28}, between the C_α atoms of the residues D23 and K28 (Figure 1). The probability distributions for the Aβ_{10-35}[D23−K28] peptides in the monomer and dimer, Aβ_{10-35}-lactam[D23−K28], and Aβ_{10-35}-lactam[D23−K28](OPLS) sample are smaller values compared to the WT Aβ_{10-35} peptide in the dimer. The distributions $P(R_g)$ for all the three systems peak at R_g between 9 and 10 Å (Figure 1c). The mean $\langle R_g\rangle$ ($= \int R_g P(R_g)\, dR_g$) of the peptide in Aβ_{10-35}[D23−K28], Aβ_{10-35}-lactam-[D23−K28], and Aβ_{10-35}-lactam[D23−K28](OPLS) is 10.3, 10.7, and 9.7 Å, respectively, while $\langle R_g\rangle$ of the monomer in the [Aβ_{10-35}[D23−K28]]$_2$ and [Aβ_{10-35}]$_2$ is 10.3 and 11.4 Å, respectively. Even though $\langle R_g\rangle$ of the Aβ_{10-35} peptide in [Aβ_{10-35}]$_2$ is nearly the same as in the Aβ_{10-35}[D23−K28] monomer, the WT monomer extensively samples conformations with R_g between 12 and 16 Å (Figure 1c).

The distributions $P(R_{ee})$ of Aβ_{10-35}[D23−K28] monomer and the Aβ_{10-35} dimer (Figure 1d) show prominent peaks at $R_{ee} \approx$ 15 and 4 Å, respectively. Aβ_{10-35} peptide has hydrophobic residues, Y10 and V12, at the N-terminus, while the C-terminus contains I31/32, L34, and M35. The conformations with low R_{ee} are due to the favorable interactions of the hydrophobic residues at the two termini. The peaks at $R_{ee} \approx 15$ Å in the $P(R_{ee})$ of monomer Aβ_{10-35}[D23−K28] and the one at $R_{ee} \approx 4$ Å in [Aβ_{10-35}]$_2$ arise from contacts between the N-terminal residues Y10, E11, and V12 and the C-terminal residues A30, I31, I32, L34, and M35. The distribution of $P(R^{\alpha}_{23-28})$, which

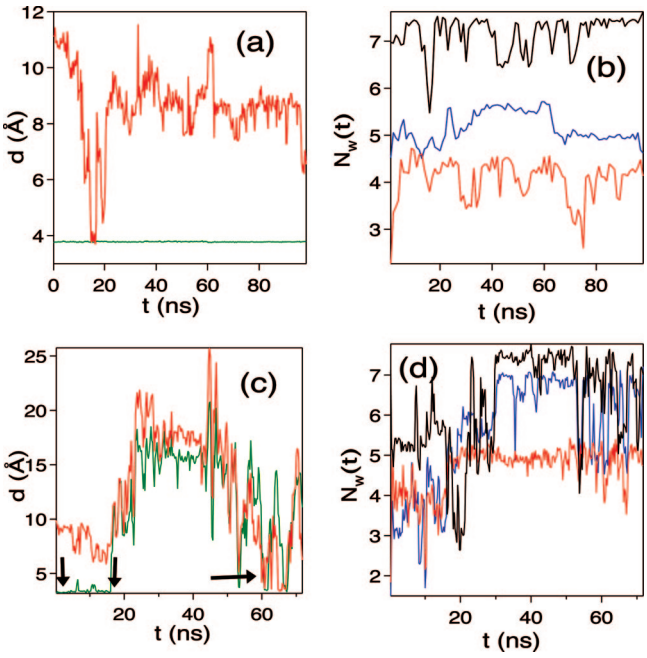

Figure 2. (a) Time-dependent changes in the salt bridge distances in the Aβ_{10-35}[D23−K28] monomer. Green and red lines show the data for D23−K28 and E22−K28 salt bridge, respectively. (b) Number of water molecules within 3.5 Å of the salt bridge forming atoms of residues E22, D23, and K28 in the Aβ_{10-35}[D23−K28] monomer. Black, blue, and red lines show the data for residues E22, D23, and K28, respectively. (c) Time-dependent changes in the salt bridge distances in WT Aβ_{10-35} monomer. Two arrows pointing downward point to the 17 ns time interval during which the D23−K28 salt bridge is kinetically stable. Arrow pointing to the right shows the reformation of the salt bridges after nearly 60 ns. Color codes are the same as in (a). (d) Number of water molecules within 3.5 Å of the salt bridge forming atoms of residues E22, D23, and K28 in WT Aβ_{10-35} monomer. Color codes are the same as in (b). The number of water molecules is averaged over 0.25 ns.

shows the stability of the bend comprising of residues 23−28, reveals that constraining the peptides by a harmonic force or by lactam bond forces it to sample conformations with compact bends (Figure 1e). The distances in the bend-stabilized conformations with R^{α}_{23-28} in the 4−8 Å range are rarely sampled by the WT Aβ_{10-35} peptides.

E22−K28 Salt Bridge Is Unstable in Aβ_{10-35}[D23−K28]. The formation of D23−K28 and E22−K28 salt bridges is probed by the time-dependent changes in the distance between the C_δ atom of E22 and N_ζ atom of K28 and the distance between the C_γ atom of D23 and N_ζ atom of K28 (Figure 1a). The harmonic constraint forces the D23−K28 salt bridge to remain stable. However, even with the constraint, the E22−K28 salt bridge is unstable (Figure 2a). Figure 2b shows the number of water molecules, N_w, near the C_δ atom of E22, C_γ atom of D23, and N_ζ atom of K28 in Aβ_{10-35}[D23−K28] as a function of time. Because of the harmonic constraint, the number of water molecules near K28 does not vary significantly as the E22−K28 salt bridge breaks and forms (Figure 2b). As the E22−K28 salt bridge forms between 15 and 20 ns, the number of water molecules near the C_δ atom of residue E22 decreases (Figure 2b). The anticorrelation between the occupancy of water near the charged residues and the propensity to form salt bridges shows that desolvation barrier prevents spontaneous interaction between E22−K28 even though K28 is spatially localized.

Charged residues in Aβ_{10-35}[D23−K28] remain solvated. The harmonic constraint on the D23−K28 salt bridge in the monomer, which stabilizes the bend structure comprising of residues 23−29, does not render the D23−K28 salt bridge inaccessible to water. The average number of water molecules, $\langle N_w \rangle$, near the salt bridge forming atoms of residues E22, D23, and K28 from the three simulations of Aβ_{10-35}[D23−K28] are 6.7, 5.1, and 4.4, respectively. These results are in accord with the previous study[7] that showed in the WT Aβ_{10-35} residues D23 and K28 make stronger contacts with water than water with itself. Moreover, D23 forms a greater number of contacts with water than K28. The values of $\langle N_w \rangle$ near the E22, D23, and K28 in the WT Aβ_{10-35} dimer are 6.7, 6.1, and 4.8, which are similar to that found in the Aβ_{10-35}[D23−K28] monomer. We conclude that the residues D23 and K28 in the Aβ_{10-35}[D23−K28] monomer, with a stable bend structure formed by the residues 23−29, remain solvated. Thus, the enhanced fibril formation rate in Aβ_{1-40}-lactam[D23−K28] conformer relative to the WT is not merely due to a significant decrease in the desolvation barrier.

Influence of Interpeptide Interactions in WT[Aβ_{10-35}]$_2$ on the Stability of E22−K28 and D23−K28 Salt Bridges. Because the intra-peptide D23−K28 salt bridge is solvated in the isolated monomer and in Aβ_{10-35}[D23−K28], it follows that the dehydration of the salt bridge must arise from inter-peptide interactions. To assess the extent to which inter-peptide interactions render the salt bridges stable, we generated three 70 ns trajectories with dimers with a preformed D23−K28 salt bridge. In the three simulations in which we monitor the stability of the salt bridges in the six peptides, the distance between the salt bridge forming atoms (Figure 1a) in five monomers increases in less than 8 ns (data not shown). In one of the peptides, the D23−K28 salt bridge is metastable for about 17 ns, which is long enough to probe the factors that contribute to its transient stability (Figure 2c). The distance (R_{sb}) between the salt bridge forming atoms, C_γ of residue D23 and N_ζ of residue K28 (Figure 2c), hops between 3 Å (salt bridge intact) and 15−20 Å (absence of salt bridge). The hop correlates with solvation which is indicated by the increase in the number of water molecules near D23 and K28 (Figure 2d). As the salt bridge reforms after 60 ns, there are fluctuations in the number of water molecules near D23 and E22 due to the exchange of water molecules between the bulk and the vicinity of the salt bridge. A representative structure of the dimer (Figure 3a) shows that the kinetic stability of the D23−K28 salt bridge (Figure 2c) in one monomer is due to the shielding of the salt bridge from water molecules by the other monomer. The D23−K28 salt bridge comes out from the plane of the bend, encompassed by residues 22−29, and is close to the second monomer which prevents water molecules from solvating the salt bridge. The shielding of water can be inferred by comparing the radial distribution function between the C_γ atom of residue D23 and the water oxygen atoms when the D23−K28 salt bridge is kinetically stable between 0 and 17 ns and when the salt bridge is broken between 34 and 46 ns (Figure 3b). In the conformation with the intact salt bridge, the solvent is depleted near D23.

Comparison of the distributions $P(R_{sb})$ of the salt bridge distances, R_{sb}, in the WT Aβ_{10-35} and the Aβ_{10-35}[D23−K28] peptides shows that the probability of formation of the E22−K28 salt bridge increases in Aβ_{10-35}[D23−K28] (Figure 4). We calculated $P(R_{sb})$ by averaging the data from both the Aβ_{10-35}[D23−K28] monomer and the dimer simulations. The probability for the formation of the E22−K28 salt bridge is negligible in the WT peptides.

From the set of Aβ_{10-35} simulations, we conclude that the stability of the D23−K28 salt bridge requires (a) the charge residues be desolvated and (b) the conformational fluctuations

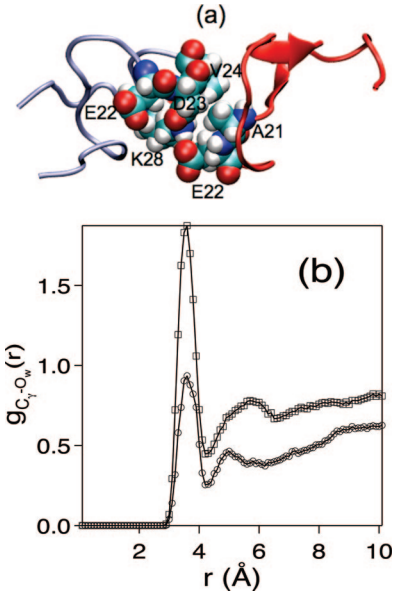

Figure 3. (a) Structure from the WT [Aβ_{10-35}]$_2$ simulation. The stable salt bridge between D23 and K28 in the monomer on the left (cyan) is shielded from the water molecules by the monomer on the right (red). Figures are prepared using VMD.[51] (b) Radial distribution function between C_γ atom of residue D23 (Figure 1a) and the water oxygen atoms. Plot in circles is obtained by averaging the data from 0−12 ns during which the D23−K28 salt bridge is stable, and the plot in squares is obtained by averaging the data from 34−46 ns where the D23−K28 salt bridge is ruptured (Figure 2c). When the salt bridge is intact, it is in a dehydrated environment.

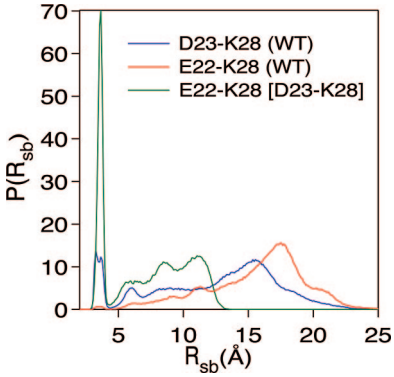

Figure 4. Probability distribution of the D23−K28 and E22−K28 salt bridge distances. Here R_{sb} is the distance between the salt bridge forming atoms of residues D23 and K28 in the case of D23−K28 salt bridge and the distance between the salt bridge forming atoms of residues E22 and K28 for the E22−K28 salt bridge. Atoms engaged in salt bridge are the C_δ atom of residue E22, C_γ atom of residue D23, and N_ζ atom of residue K28 (Figure 1a). Blue, red, and green lines represent the data for D23−K28 salt bridge in WT Aβ_{10-35}, E22−K28 salt bridge in WT Aβ_{10-35}, and E22−K28 salt bridge in Aβ_{10-35}[D23−K28], respectively. The sharp peak in the green curve shows that constraining the D23−K28 distance enhances the probability of forming the E22−K28 interaction.

be suppressed by inter-peptide interactions. The second requirement ensures that the charged residues are prevented from being solvent exposed. Clearly, dimer is not large enough to satisfy both the requirements. It is likely that only after the size of the oligomer exceeds the critical nucleus is the salt bridge with an intact bend stable.

Conformational Fluctuations in Aβ_{10-35}[D23−K28] and Aβ_{9-40}[D23−K28] Are Similar. In order to assess whether the instability of the E22−K28 contact and the structural features of Aβ_{10-35}[D23−K28] are a consequence of the size of the

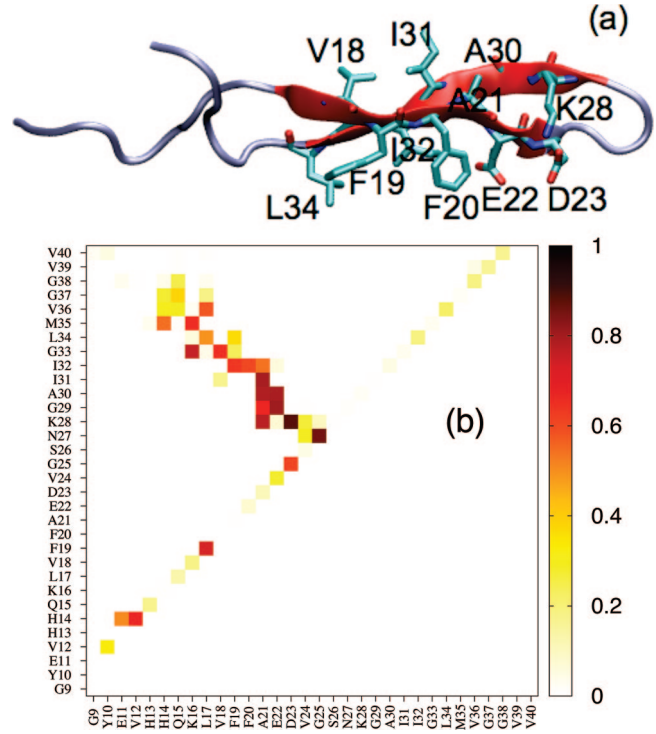

Figure 5. (a) Snapshot of a Aβ_{9-40}[D23−K28] monomer where the C- and N-terminal hydrophobic residues interact to form β-sheet. This assembly competent structure, labeled as N*, is similar to that found in the fibril. (b) Contact map of the Aβ_{9-40}[D23−K28] monomer obtained by averaging 15 ns of the trajectory from which the structure in (a) is taken. Monomers are in contact if the center of mass of two residues is ≤6 Å.

monomer, we also performed limited simulations of the Aβ_{9-40}[D23−K28] monomer. It is suspected that the monomers of Aβ_{10-35} in its fibril would be arranged in parallel[16] as in the fibrils of Aβ_{1-40}. In the TM, the first nine residues in the N-terminus are disordered, and the monomer is stabilized by hydrophobic interactions between the residues in the N- and C-termini and the salt bridge D23−K28. In the Aβ_{10-35}, the C-terminus is shorter. Nevertheless, similar forces are expected to stabilize the fibril, thus making Aβ_{10-35} a good model for Aβ_{1-40}.

Using the initial conformation of the Aβ_{9-40} monomer from the fibril structure, we produced three 15 ns trajectories by constraining the D23−K28 salt bridge by a harmonic potential (see Methods). In all the three trajectories, the monomer forms kinetically stable structures similar to the one in Figure 5a. The hydrophobic patches near the N- and C-termini, which form extended β-strands, interact to form β-sheets. The constrained D23−K28 salt bridge is perpendicular to the bend formed by residues D23 to K28 and is not buried inside the loop (Figure 5a). Thus, the charged residues are solvated as in the Aβ_{10-35}[D23−K28] monomer. The contact map (Figure 5b), obtained by averaging over the 15 ns simulation data, shows that the hydrophobic contacts are kinetically stable. When the E22−K28 salt bridge forms, there is fluctuation in the water molecules near the C_δ atom of residue E22 (data not shown). The decrease in the number of water molecules as the salt bridge forms is in agreement with the Aβ_{10-35} simulations. The average number of water molecules, $\langle N_w \rangle$, near the salt bridge forming atoms of residues E22, D23, and K28 from the three trajectories of Aβ_{9-40}[D23−K28] are 6.6, 5.3, and 4.5, respectively. The values of $\langle N_w \rangle$ near the E22, D23, and K28 in the Aβ_{10-35}[D23−K28] monomer are 6.7, 5.1, and 4.4, which are

similar to that found in the $A\beta_{9-40}$[D23−K28] monomer. These results show that the major conclusions found in the more extensive simulations of $A\beta_{10-35}$[D23−K28] monomer are consistent with those found for $A\beta_{9-40}$[D23−K28] as well.

Stability of Assembly Competent N* Structures Require Interactions between Extended N- and C-Termini Strands. A possible explanation for the enhanced fibril formation rate of the $A\beta_{1-40}$-lactam[D23−K28] is that the structures that are frequently sampled in this congener is fibril-like. In other words, the N* structure is similar to the one the monomer adopts in the fibrils. In order to shed light on the factors that stabilize the fibril-like N* structures, those with β-strands in the residues near the N- and C-termini connected by a stable bend with the D23 and K28 close enough to engage in salt bridge formation (see Figure 5a), we performed a number of simulations for the WT $A\beta_{9-40}$ monomer. In the first, the initial conformations for the MD simulations are taken from the end point of the $A\beta_{9-40}$[D23−K28] calculations. Starting from the initial structures that are similar to that in Figure 5a, we generated three independent 15 ns trajectories. In all cases, the D23−K28 salt bridge is kinetically stable, and the fluctuation in the number of water molecules near the salt bridge is similar to that in $A\beta_{10-35}$[D23−K28] and $A\beta_{9-40}$[D23−K28] simulations (data not shown). We surmise that the salt bridge stability in the WT $A\beta_{9-40}$ monomer is due to favorable (largely hydrophobic) intrastrand interactions.

To further test the proposal that favorable intrapeptide strand−strand interactions can stabilize the N* structures, we performed WT monomer simulations in which the initial conformations are taken from the TM model and other conformations which have D23−K28 salt bridge but without the hydrophobic interaction between the residues present at the N- and C-termini. In all trajectories, the distance between D23−K28 and E22−K28 increased (data not shown) when there are no hydrophobic interactions between the residues present at the N- and C-termini. Thus, these potential salt bridges are unstable, and the WT monomer adopts a collapsed coil structures without significant interactions between the N- and C-termini.

In order to ascertain whether a stable D23−K28 salt bridge is necessary, in addition to the hydrophobic interactions between the C- and N-terminal residues to the stability of conformers similar to the one shown in Figure 5a, we mutated the D23 residue to A23 and generated three trajectories each 12 ns long. These simulations are intended to ascertain the kinetic stability of the mutated conformations. The contact map (data not shown) obtained by averaging over the 12 ns simulation data of one of the runs shows that the hydrophobic contacts are kinetically stable without the D23−K28 salt bridge when compared to the contact map (Figure 5b). The contact maps C_1 and C_2 will be identical if the contact values at $C_1(i, j)$ and $C_2(i, j)$ are similar. The similarity between contact maps C_1 and C_2 can be assessed by taking the dot product between the maps. The contact maps of size $k \times l$ can be represented as a vector of length $n = k \times l$. These vectors are normalized, and a dot product is taken between the vectors. The maximum value of 1 indicates high similarity between the contact maps. The dot product between the contact map (Figure 5a) and the contact maps of the three trajectories obtained by mutating D23 residue to A23 are 0.9, 0.91, and 0.87, respectively. The root-mean-square deviation (rmsd) deviation plot of the mutated monomer with respect to the initial conformation as a function of time (data not shown) shows that the structures are stable without the D23−K28 salt bridge. These results show that the hydrophobic interactions between the C- and N-terminal residues play a major role in stabilizing the fibril-like, N* species. The high value of the dot product and stable rmsd values show that the hydrophobic contacts are the key for the stability of the conformers of the type shown in Figure 5a.

Taken together, these results show that the predominant driving force for the formation of N* structures is the interaction of the hydrophobic residues at the N- and C-termini that leads to a β-sheet like structure. In such a structure, the formation of D23−K28 salt bridge is inevitable. If D23−K28 salt bridge is constrained, as in $A\beta_{1-40}$-lactam[D23−K28] structure, then N- and C-termini interactions are encouraged, thus leading to the formation of FL conformations that can self-assemble rapidly.

Average Monomer Structures of $A\beta_{10-35}$[D23−K28] and $A\beta_{9-40}$[D23−K28] Are Similar and Fibril-like. The structure of the $A\beta_{1-40}$ in the TM[13,14] has two β-strand segments, comprising residues 10−22 and 30−40, along with a bend involving residues 23−29. The monomer is stabilized by an intramolecular interface formed by contacts between residues 19−20 and 33−35 and the D23−K28 salt bridge. The ensemble of low-energy structures of $A\beta_{10-35}$[D23−K28] and $A\beta_{9-40}$[D23−K28] monomer has a similar backbone topology as the $A\beta_{1-40}$ monomer in the TM. In other words, the fibril-like, N* structures are already preformed in the monomer. These structures are stabilized by interactions between the hydrophobic residues in the N and C terminals (Figures 5a and 6a). The N-terminal residues of the monomers 10−13 are in contact with the C-terminal residues 29−35 along with the bend formed by the residues 22−29. Structures with similar topologies are also observed in the oligomer simulations of $A\beta_{1-40}$ and $A\beta_{10-35}$ performed using coarse-grained[24] and atomistic description[25] of the peptides in implicit solvent.

Globally, the $A\beta_{10-35}$[D23−K28] is compact. Both R_{ee} and R_g (Figure 6b) show that the monomer stretches completely between 10 and 20 ns and then collapses to a structure where the C-terminal and the N-terminal residues are in proximity to form a β-sheet. The contact map in Figure 6c shows that there are two regions in the map where the nonbonded contacts dominate. One is in the bend region consisting of residues 20−29, and the other region is between the terminal ends of the protein consisting of residues 10−13 and 30−35. The peptide in this conformation is stabilized by contacts, especially at the terminal ends between residues 10 and 30 and between residues 11 and 32. The contacts in the bend region are between residues 20 and 28, 23 and 25, and 23 and 28. This structure satisfies PASA because in this conformation the number of intramolecular hydrophobic contacts is maximized and the potential frustration of burying the charged interaction is eliminated.

The secondary structure analysis using STRIDE[41] shows that there is negligible helical content. The residues with the largest β-strand contacts calculated by using time averages are E11 (49%), V12 (3%), I32 (38%), G33 (13%), and L34 (2%). The overall structure of the $A\beta_{10-35}$[D23−K28] monomer and the topology of the same region in the $A\beta_{1-40}$ amyloid fibril are strikingly similar. We conclude that the D23−K28 constraint populates an ensemble of structurally related N* conformations that is poised to aggregate.

Comparison of Energy Landscapes of $A\beta_{10-35}$ and $A\beta_{10-35}$[D23−K28] Reveal Enhanced Population of N* Species in $A\beta_{10-35}$[D23−K28]. A visual representation of the most populated basins can be obtained by projecting the energy landscape along the lowest eigen values of the principal component analysis[42] based on the dihedral space (see Methods). The energy landscape of the $[A\beta_{10-35}]_2$ (Figure 7a), $A\beta_{10-35}$-

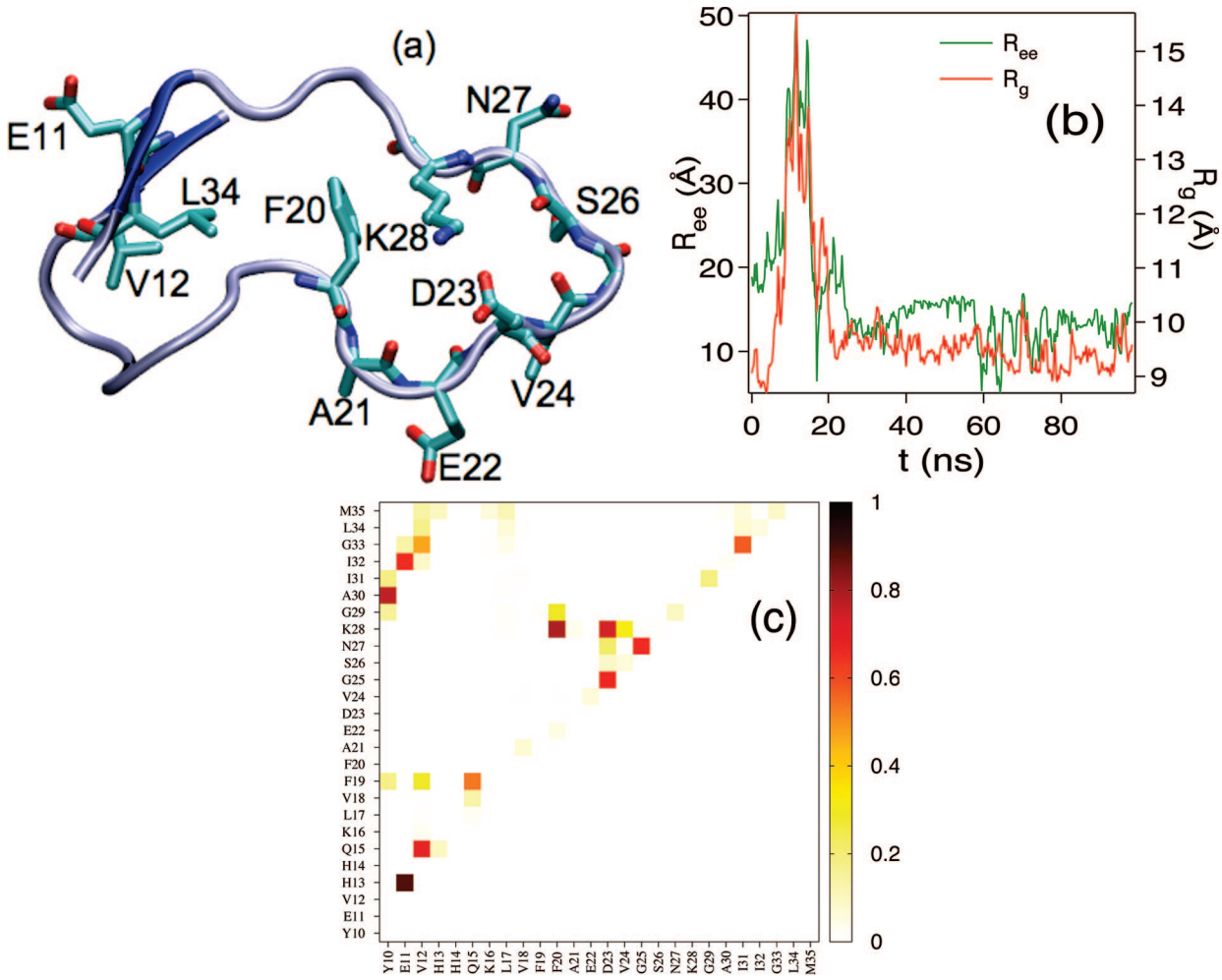

Figure 6. (a) Structure of the N* state of Aβ_{10-35}[D23−K28] monomer. There are a lot of similarities between the N* conformation and the structure of the monomer in the model fibril structure. Residues D23 and K28, which form the salt bridge, and the C and N terminal hydrophobic residues E11, V12, and L34 are in contact. (b) R_g and R_{ee} as a function of time of the monomer. The peptide is compact and samples manifolds of collapsed structures (see Figure 1). (c) Contact map of the monomer obtained by averaging 40−100 ns of the trajectory from which the structure in (a) is taken. Monomers are in contact if the center of mass of two residues is ≤6 Å.

[D23−K28] (Figure 7b), and [Aβ_{10-35}[D23−K28]]$_2$ (Figure 7c) shows that a number of basins are sampled. However, for the systems with intact D23−K28 salt bridge the aggregation prone N* structure is populated with substantial probability. Because population of the N* is required for oligomerization to begin, it follows that the aggregation should occur more easily in Aβ_{10-35}[D23−K28] than in the wild type. The energy landscape provides a clear pictorial view of the importance of the N* in triggering aggregation.

Secondary Structural Fluctuations in WT Aβ_{10-35} and Aβ_{10-35}[D23−K28] Peptides. It is clear from the present and previous studies that the structures in WT Aβ_{10-35} and Aβ_{9-40} sample conformations in an energy landscape with a number of distinct basins. Simulations[10,43] show that, in some of these structures, there are stretches that have helical or β-strand content. Our simulations of [Aβ_{10-35}]$_2$ also show that there is a propensity for the residues 19−24 to form an α-helix (Figure 8). The structures with intact α-helix, in the 19−24 region, disrupts bend between 22 and 29. When the residue D23 is part of the helix, the bend is destabilized. More importantly, upon stabilizing the D23−K28 salt bridge with a harmonic constraint, the fluctuating helix is not observed in the simulations involving Aβ_{10-35}[D23−K28] (data not shown). The limited set of simulations on Aβ_{10-35}-lactam[D23−K28] and Aβ_{10-35}-lactam-[D23−K28](OPLS) also show that the helix propensity of residues 19−24 is negligible. However, in the Aβ_{10-35}-lactam[D23−K28](OPLS) peptide, residues 16−18 (7.8%) and residues 25−28 (16.3%) have non-negligible helix propensity. While the details can depend on force fields, a benchmark study[44] concluded that the prediction made by the CHARM22 force field is in good agreement with experiments in predicting helices at the correct positions in the proteins.

It is suggested from previous studies[43,46,47] that the disruption of the helical fragments in the middle of the peptide decrease the barriers to protein aggregation. Mass spectroscopy experiments[47] on Aβ_{1-40} suggest that the protease resistant peptide segment formed by residues 21−30 plays a key role in the nucleation of the aggregation process. Recent simulations[43] suggested that the increased rates of Aβ aggregation, at pH = 6, might be due to the decrease in helical propensity of the residues 17−22. Mutations[46] of residue E22Q which reduced the propensity of helix formation in this region also increased the rate of Aβ amyloid formation.

In contrast, in the Aβ_{10-35}[D23−K28] congener, harmonic potential greatly destabilizes the fluctuating helix formed by residues 19−24 and stabilizes the bend formed by the residues 23−29 to produce the aggregation prone N*. In Aβ_{10-35}-[D23−K28], conformations with intramolecular contacts among the hydrophobic residues present in the N- and C-terminals form with high propensity. Frequent sampling of such conformations,

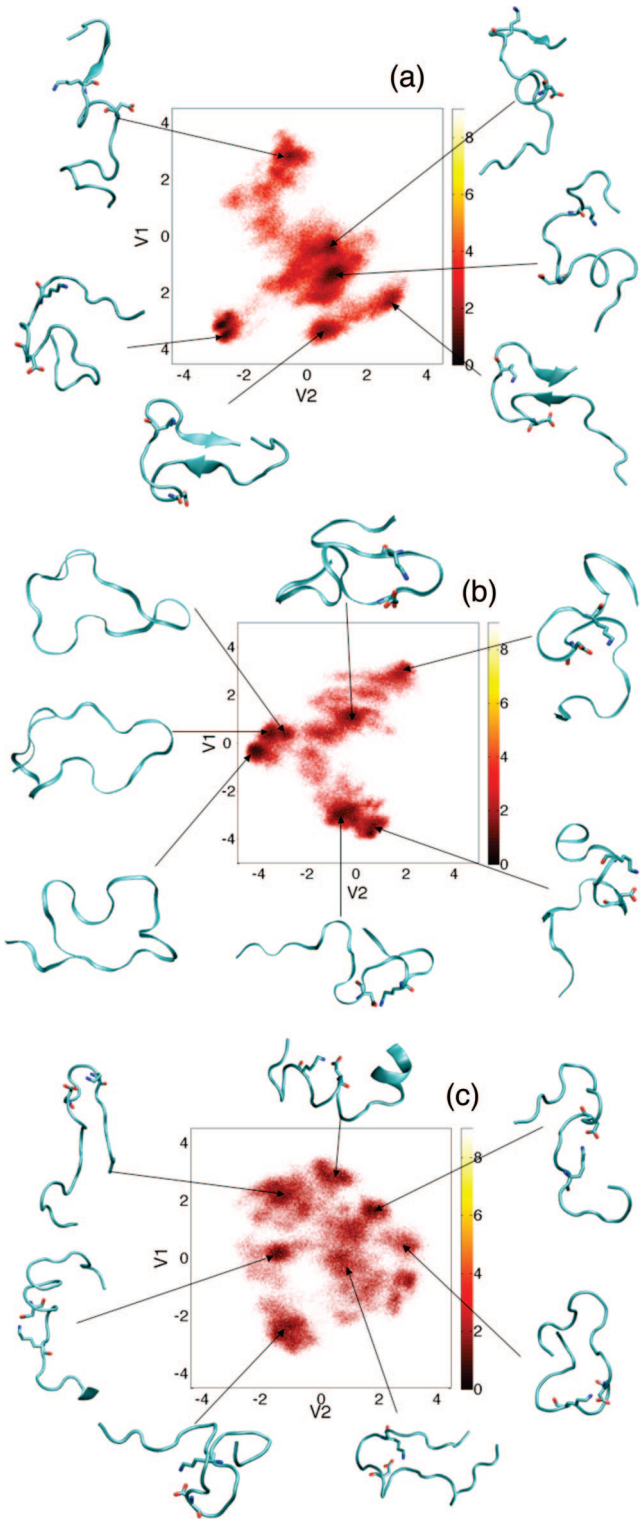

Figure 7. Projection of the free energy landscape for the Aβ_{10-35} monomer on to the lowest two eigenvectors of the dihedral principal component analysis. The scale for the free energy in units of k_BT, where k_B is the Boltzmann constant and T is the temperature, is given on the right. (a) Wild type dimer. (b) Monomer Aβ_{10-35}[D23−K28]. (c) Dimer Aβ_{10-35}[D23−K28].

which are similar to the peptide conformations in the model amyloid fibril, due to the decrease in conformational entropy compared to the WT peptide could be the reason for the increased rates of aggregation observed in experiments[29] when the D23−K28 salt bridge is constrained by a lactam molecule (see below).

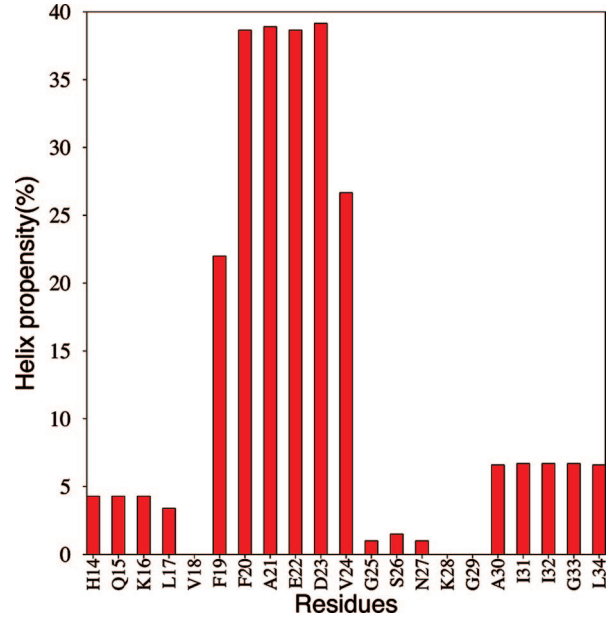

Figure 8. Helical propensity of residues in dimer simulations of the WT Aβ_{10-35}. The percentage propensity is calculated by using N_H^k/N_T, where N_H^k is the number of conformations in which residue k forms a helix and N_T is the total number of conformations obtained. We used the criterion given in STRIDE[41] to ascertain if a residue is in a helical conformation.

Discussion

Importance of N*. The Aβ_{10-35} and Aβ_{9-40} monomers in the WT can be viewed as an ensemble of compact conformations with fluctuating residual structures in different regions. The structures can be clustered into distinct basins.[7,8,10] Structures in the most populated Aβ monomer basins are not assembly competent. However, due to the random-coil nature, the peptides also sample conformations in basins with high free energy. A class of high free energy assembly competent structures can collide to form oligomers that can nucleate and grow.[28] Here, we have shown that such fibril-like (referred to as N*) that are metastable in the WT structures are similar to the monomers in the amyloid fibril. The N* conformations are heterogeneous and are stabilized by favorable hydrophobic interactions between N- and C-terminal residues provided they are arranged in β-strand conformations. The two strands are connected by a bend involving residues 23−29. The geometry of the N* structure brings D23 and K28 in proximity so that they can form a salt bridge with a bend involving residues 23−29 (Figure 5a).

The basic picture of the assembly of the WT Aβ peptides that emerges from this study and earlier all atom simulations[7,9,10] and the more recent lattice model simulations[48] is the following (Figure 9). The limited number of assembly competent structures, N*, are only populated due to fluctuations and denaturation stress. If a pair of such N* molecules collide, they can form dimers, which can recruit additional N* molecules to form higher order structures. The oligomers of N* molecules, $(N^*)_n$, undergo substantial structural fluctuations as an additional disordered molecule is added to form[38] $(N^*)_{n+1}$. Only when n exceeds the critical nucleus size, which is expected[38,49] to be about 8−10, do these oligomers rearrange to form protofilaments and fibrils. In the process of fibril formation, N* rearranges further and is stabilized by both inter- and intra-peptide interactions. Mutations or lactam bridges that enhance the formation of N* in the monomer would increase the aggregation rates.

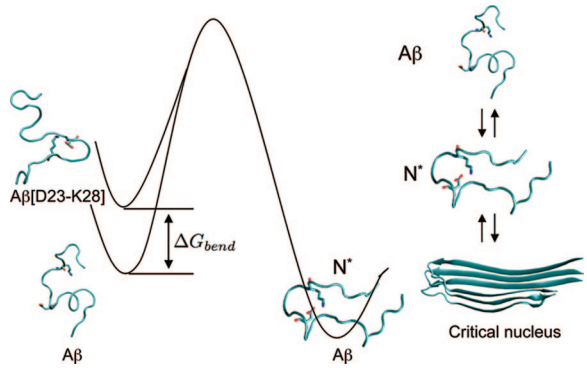

Figure 9. Schematic free energy profile for the conversion of Aβ and Aβ[D23−K28] to assembly competent N* structure. Although we have shown only a single structure for the unfolded conformation, it should be stressed that both the WT and Aβ[D23−K28] sample a number of distinct conformations. Thus, these structures as well as N* should be viewed as an ensemble. The rates of nucleus formation are dependent on the ease of populating the assembly competent N* structure. Both mutations and preformed salt bride can decrease the barrier to N* formation. On the right a schematic for the aggregation mechanism is presented. The Aβ peptide transiently populates the assembly competent N* structure. These N* structures collide to form the critical nucleus that can subsequently grow to form protofilaments and fibrils.

Increasing the population of N* conformations requires structural changes in the collapsed coils. First, the N and C terminal hydrophobic residues have to be largely in a β-strand conformation to initiate the formation of an overall β-sheet structure.[50] Second, the orientation of the bend relative to the strands should facilitate the D23−K28 salt bridge formation. In the Aβ_{10-35}[D23−K28] and Aβ_{9-40}[D23−K28] the salt bridge is preformed although the charged residues are still solvated. The decrease in the conformational entropy in these monomers facilitate the formation of the β-strands and hence the N* species. These structural changes involve overcoming both entropic and enthalpic barriers. As a result, the N* conformation is not significantly populated in the WT Aβ peptides. However, the high free energy fibril-like N* conformations in the Aβ monomer can be stabilized by a affibody protein ($Z_{A\beta3}$) that can stabilize N* and prevent it from aggregation.[50] The NMR structure of $Z_{A\beta3}$−Aβ complex further supports the importance of N* identified here as an important monomeric conformation that promotes fibril formation.

Reduction in Entropic Barrier in the Formation of N* in Lactam Construct. Because the D23 and K28 residues are in a dehydrated environment in the fibril, it is tempting to suggest that the kinetic barrier to desolvating these charged residues could explain the slow fibril formation rate in the WT. Our simulations suggest that the formation of β-strands involving N and C termini residues, and their interaction represents the crucial kinetic step in generating N* structures. The reduction in the conformational entropy in the Aβ_{10-35}[D23−K28] monomer decreases the barrier to β-strand formation and hence can lead to a significant probability of N* formation. The N* species whose structure in complex with affibody has been determined by NMR[50] adopts a hairpin-like conformation. A similar hairpin-like structure is observed in our simulations of the Aβ_{10-35}[D23−K28] monomer (Figure 6a). Thus, one can estimate the reduction in the free energy barrier to N* formation in the lactam-Aβ congener by estimating the free energy cost to form a bend in the WT Aβ (see Figure 1e). Since we postulate that hairpin-like structure of Aβ peptide is aggregation prone, then any mutations or constraints in the peptide which enhance the formation of this structure should speed up the aggregation process. If we assume that the decrease in free energy barrier in the Aβ_{10-35}-lactam[D23−K28] is solely related to the bend formation, then $\Delta G^{\dagger}/k_BT = -\ln(k_{[D23-K28]}/k_{WT}) \approx \Delta G_{bend}/k_BT$ (Figure 9). Here k_{WT} and $k_{[D23-K28]}$ are the rate constants for the N* formation in the wild type and the D23−K28 salt bridge constrained monomer, k_B is the Boltzmann constant, and T is the temperature. It is reasonable to assume that free energy (ΔG_{bend}) cost of bend formation is one of the major differences in the rates of the hairpin-like structure formation in these two species. Then, free energy for the bend formation from experiments is given by $k_BT \ln(k_{[D23-K28]}/k_{WT}) = k_BT \ln(1000) = 6.9k_BT$.

TABLE 1: Free Energy Cost for Bend Formation in Aβ Peptides

Aβ D23−K28 salt bridge constrained peptides	$\langle R^{\alpha}_{23-28}\rangle^a$ (Å)	$\Delta G_{bend}/k_BT^b$
Aβ_{10-35}[D23−K28]	6.6	6.9
Aβ_{10-35}[D23−K28]$_2$	8.1	3.4
Aβ_{10-35}-lactam[D23−K28]	7.2	5.4
Aβ_{10-35}-lactam[D23−K28](OPLS)	7.9	3.6
$\langle R^{\alpha}_{23-28}\rangle$ of the four above species averaged	7.5	4.6

[a] $\langle R^{\alpha}_{23-28}\rangle = \int R^{\alpha}_{23-28} P(R^{\alpha}_{23-28})\, dR^{\alpha}_{23-28}$, where $P(R^{\alpha}_{23-28})$ is the distribution of the distance between the α-carbon atoms of D23 and K28. [b] The free energy cost for forming a bend (a hairpin-like structure) in WT is given by eq 1.

Using our simulations, we can estimate ΔG_{bend} involving residues 23−28 using the distance between the C_α atoms of D23 and K28 as an order parameter. Using the probaility distribution of $P(R^{\alpha}_{23-28})$, where R^{α}_{23-28} is the distance between the C_α atoms of the residues D23 and K28 (Figure 1e), the calculated mean $\langle R^{\alpha}_{23-28}\rangle$ ($= \int R^{\alpha}_{23-28} P(R^{\alpha}_{23-28})\, dR^{\alpha}_{23-28}$) for various D23−K28 salt bridge constrained Aβ peptides is given in Table 1. The values of ΔG_{bend} is calculated from the wild type Aβ_{10-35} dimer data for $P(R^{\alpha}_{23-28})$ using

$$\Delta G_{bend} = -k_BT \log\left(\frac{P(R^{\alpha}_{23-28} < \langle R^{\alpha}_{23-28}\rangle)}{P(R^{\alpha}_{23-28} > \langle R^{\alpha}_{23-28}\rangle)}\right) \qquad (1)$$

where $P(R^{\alpha}_{23-28} < \langle R^{\alpha}_{23-28}\rangle) = \int_0^{\langle R_{23-28}{}^{\alpha}\rangle} R^{\alpha}_{23-28} P(R^{\alpha}_{23-28})\, dR^{\alpha}_{23-28}$ and $P(R^{\alpha}_{23-28} > \langle R^{\alpha}_{23-28}\rangle) = \int_{\langle R_{23-28}{}^{\alpha}\rangle}^{\infty} R^{\alpha}_{23-28} P(R^{\alpha}_{23-28})\, dR^{\alpha}_{23-28}$. ΔG_{bend} estimated from WT and various D23−K28 salt bridge constrained Aβ peptides is given in Table 1. The free energies estimated are in the range (4−7)k_BT. Thus, a large decrease in barrier ($\approx\Delta G_{bend}$) to N* conformation occurs upon using the lactam construct which explains the enhancement in the aggregation of Aβ peptides with preformed salt bridge between D23 and K28. It should be stressed that the estimates made here explain only qualitatively the origin of enhanced fibril growth rate in the lactam construct. The transition from dimers to protofilaments and fibrils is a complex process. Undoubtedly, a number of other factors play a role in the rate of growth of the amyloid fibril.

Dependence of the Results on Force Field. To ensure that the major conclusions of our simulations are robust, we have also performed a limited set of Aβ_{10-35}-lactam[D23−K28] monomer simulations using all atom OPLS force field.[34] It is instructive to compare the results obtained using the two force fields.

1. The Aβ_{10-35}-lactam[D23−K28](OPLS) peptide samples compact conformations (in agreement with the Aβ_{10-35}-[D23−K28] and Aβ_{10-35}-lactam[D23−K28] peptides) compared

to the wild type Aβ_{10-35} peptide. The probability distributions of R_g, R_{ee}, and R^{α}_{23-28} sample smaller values compared to the WT Aβ_{10-35} peptide (Figure 1). These results are qualitatively similar to that found using CHARMM force field.

2. Because of the lactam construct, the salt bridge forming atoms C_γ atom of residue D23 and N_ζ atom of residue K28 are not charged. There is a neutral amide bond between the β-carbon of Asp23 and ϵ-carbon of Lys28. So the salt bridge forming atoms are desolvated compared to the WT or the Aβ_{10-35}[D23−K28] peptides, which have charged salt bridge forming atoms that can interact with water. Residue E22 in Aβ_{10-35}-lactam[D23−K28] or Aβ_{10-35}-lactam[D23−K28]-(OPLS) cannot form a salt bridge, since residue K28 is not charged in the lactam construct. Since residue E22 is charged, it is solvated in the lactam construct. The average number of water molecules near the salt bridge forming atoms of residue E22, D23, and K28 in peptide Aβ_{10-35}-lactam[D23−K28]-(OPLS) is 5.6, 1.4, and 1.7. The numbers for the Aβ_{10-35}-lactam[D23−K28] peptide simulated in the CHARMM force field are 6.5, 2.7, and 2.4. The numbers for the WT dimer and Aβ_{10-35}[D23−K28] are 6.6, 5.3, and 4.5 and 6.7, 5.1, and 4.4, respectively.

3. Simulations of Aβ_{10-35} WT dimer using CHARMM force field show that there is a propensity for the residues 19−24 to form a α-helix. This fluctuating helix is not observed in the simulations of Aβ_{10-35}[D23−K28] in which the salt bridge forming atoms are harmonically constrained. The limited simulations of Aβ_{10-35}-lactam[D23−K28] also shows negligible helix propensity in agreement with the harmonic constraint simulations. Aβ_{10-35}-lactam[D23−K28](OPLS) monomer simulated in the OPLS force field also shows negligible helix propensity for residues 19−24. However, residues 16−18 (7.8%) and residues 25−28 (16.3%) have non-negligible tendency to adopt helical conformation.

4. The most crucial simulation result that was used to rationalize the enhancement of fibril formation rate in Aβ_{10-35}-lactam[D23−K28] is the estimate of ΔG_{bend} for bend formation. The estimated free energy for the bend formation in the hairpin-like structure in the WT Aβ_{10-35} peptide using the $\langle R^{\alpha}_{23-28}\rangle$ value obtained from the probability distribution of R^{α}_{23-28} (Figure 1e) in Aβ_{10-35}-lactam[D23−K28](OPLS) peptide is 3.6kT. This is comparable to the values obtained from the other D23−K28 salt bridge constrained peptides (Table 1).

The key results obtained from the two different force fields for all the constructs show that they are similar. In many cases, the results are almost in quantitative agreement with each other. The finding that there is a reduction in barrier to the formation of fibril-like N* structure is independent of the force fields. The decrease in the barrier to aggregation prone species arises solely due to the constraints (lactam and harmonic restraint) that ensures the preformation of the salt bridge between D23 and K28. Although conclusions reached here are a result of extensive simulations, the inherent limitations (inadequacy of force fields and the inability to sample all allowed conformations of the peptide and water molecules) make it likely that our results are only qualitatively correct. Nevertheless, by using simple arguments and by performing several kinds of simulations using two force fields, we believe that the major results, namely, the nature of forces that stabilize the aggregation prone N* species and the major reduction in the barrier to aggregation relative to the WT in the Aβ_{1-40}[D23−K28] being entropic in origin, are robust.

Acknowledgment. This work was supported in part by a grant from the National Institutes of Health through Grant R01GM076688-05. A portion of this research was conducted at the Center for Nanophase Materials Sciences, which is sponsored at Oak Ridge National Laboratory by the Division of Scientific User Facilities, U.S. Department of Energy through Grant CNMS2007-048. A part of the computational work was done using the resources of National Science Foundation Teragrid through Grant TG-MCB080035N.

References and Notes

(1) Glenner, G.; Wong, C. *Biochem. Biophys. Res. Commun.* **1984**, *120*, 885–890.
(2) Masters, C.; Simms, G.; Weinman, N.; Multhaup, G.; McDonald, B.; Beyreuther, K. *Proc. Natl. Acad. Sci. U.S.A.* **1985**, *82*, 4245–4249.
(3) Walsh, D.; Montero, R.; Bresciani, L.; Jen, A.; Leclercq, P.; Saunders, D. *Neurobiol. Dis.* **2002**, *10*, 20–27.
(4) Hardy, J.; Selkoe, D. *Science* **2002**, *297*, 353–356.
(5) Lambert, M.; Barlow, A.; Chromy, B.; Edwards, C.; Freed, R.; Liosatos, M.; Morgan, T.; Rozovsky, I.; Trommer, B.; Viola, K.; Wals, P.; Zhang, C.; Finch, C.; Krafft, G.; Klein, W. *Proc. Natl. Acad. Sci. U.S.A.* **1998**, *95*, 6448–6453.
(6) Gong, Y.; Chang, L.; Viola, K.; Lacor, P.; Lambert, M.; Finch, C.; Krafft, G.; Klein, W. *Proc. Natl. Acad. Sci. U.S.A.* **2003**, *100*, 10417–10422.
(7) Tarus, B.; Straub, J.; Thirumalai, D. *J. Am. Chem. Soc.* **2006**, *128*, 16159–16168.
(8) Han, W.; Wu, Y. *J. Am. Chem. Soc.* **2005**, *127*, 15408–15416.
(9) Baumketner, A.; Shea, J. *J. Mol. Biol.* **2007**, *366*, 275–285.
(10) Sgourakis, N.; Yan, Y.; McCallum, S.; Wang, C.; Garcia, A. *J. Mol. Biol.* **2007**, *368*, 1448–1457.
(11) Fawzi, N.; Phillips, A.; Ruscio, J.; Doucleff, M.; Wemmer, D.; Gordon, T. *J. Am. Chem. Soc.* **2008**, *130*, 6145–6158.
(12) Zhang, S.; Iwata, K.; Lachenmann, M.; Peng, J.; Li, S.; Stimson, E.; Lu, Y.; Felix, A.; Maggio, J.; Lee, J. *J. Biol. Chem.* **2000**, *130*, 130–141.
(13) Petkova, A.; Ishii, Y.; J, J., B.; Antzutkin, O.; Leapman, R.; Delaglio, F.; Tycko, R. *Proc. Natl. Acad. Sci. U.S.A.* **2002**, *99*, 16742–16747.
(14) Petkova, A.; Ishii, Y.; J, J., B.; Antzutkin, O.; Leapman, R.; Delaglio, F.; Tycko, R. *Biochemistry* **2006**, *45*, 498–512.
(15) Luhrs, T.; Ritter, C.; Adrian, M.; Riek-Loher, D.; Bohrmann, B.; Dobeli, H.; Schubert, D.; Riek, R. *Proc. Natl. Acad. Sci. U.S.A.* **2005**, *102*, 17342–17347.
(16) Ma, B.; Nussinov, R. *Proc. Natl. Acad. Sci. U.S.A.* **2002**, *99*, 14126–14131.
(17) George, A.; Howlett, D. *Biopolymers* **1999**, *50*, 733–741.
(18) Chaney, M.; Webster, S.; Kuo, Y.; Roher, A. *Protein Eng.* **1998**, *11*, 761–767.
(19) Li, L.; Darden, T. A.; Bartolotti, L.; Kominos, D.; Pedersen, L. *Biophys. J.* **1999**, *76*, 2871–2878.
(20) Lazo, N.; Downing, D. *Biochemistry* **1998**, *37*, 1731–1735.
(21) Buchete, N.; Tycko, R.; Hummer, G. *J. Mol. Biol.* **2005**, *353*, 804–821.
(22) Nelson, R.; Sawaya, M.; Balbirnie, M.; Madsen, A.; Riekel, C.; Grothe, R.; Eisenberg, D. *Nature (London)* **2005**, *435*, 773–778.
(23) Sawaya, M.; Sambashivan, S.; Nelson, R.; Ivanova, M.; Sievers, S.; Apostol, M.; Thompson, M.; Balbirnie, M.; Wiltzius, J.; McFarlane, H.; Madsen, A.; Riekel, C.; Eisenberg, D. *Nature (London)* **2007**, *447*, 453–457.
(24) Urbanc, B.; Cruz, L.; Ding, F.; Sammond, D.; Khare, S.; Buldyrev, S.; Stanley, H.; Dokholyan, N. *Biophys. J.* **2004**, *87*, 2310–2321.
(25) Jang, S.; Shin, S. *J. Phys. Chem. B* **2008**, *112*, 3479–3484.
(26) Krivov, S.; Karplus, M. *J. Chem. Phys.* **2002**, *117*, 10894–10903.
(27) Kumar, S.; Ma, B.; Tsai, C.; Sinha, N.; Nussinov, R. *Protein Sci.* **2000**, *9*, 10–19.
(28) Thirumalai, D.; Klimov, D.; Dima, R. *Curr. Opin. Struct. Biol.* **2003**, *13*, 146–159.
(29) Sciarretta, K.; Gordon, D.; Petkova, A.; Tycko, R.; Meredith, S. *Biochemistry* **2005**, *44*, 6003–6014.
(30) Borreguero, J.; Urbanc, B.; Lazo, N.; Buldyrev, S.; Teplow, D.; Stanley, H. *Proc. Natl. Acad. Sci. U.S.A.* **2005**, *102*, 6015–6020.
(31) Cruz, L.; Urbanc, B.; Borreguero, J.; Lazo, N.; Teplow, D.; Stanley, H. *Proc. Natl. Acad. Sci. U.S.A.* **2005**, *102*, 18258–18263.
(32) Phillips, J. C.; Braun, R.; Wang, W.; Gumbart, J.; Tajkhorshid, E.; Villa, E.; Chipot, C.; Skeel, R. D.; Kale, L.; Schulten, K. *J. Comput. Chem.* **2005**, *26*, 1781–1802.
(33) Mackerell, A. *J. Phys. Chem. B* **1998**, *102*, 3586–3616.
(34) Kaminski, G.; Friesner, R.; Tirado-Rives, J.; Jorgensen, W. *J. Phys. Chem. B* **2001**, *105*, 6474–6487.
(35) Darden, T.; Perera, L.; Li, L.; Pedersen, L. *Structure* **1999**, *7*, R55−R60.

(36) Martyna, G.; Tobias, D.; Klein, M. *J. Chem. Phys.* **1994**, *101*, 4177–4189.

(37) Feller, S.; Zhang, Y.; Pastor, R.; Brooks, B. *J. Chem. Phys.* **1995**, *103*, 4613–4621.

(38) Nguyen, P.; Li, M.; Stock, G.; Straub, J.; Thirumalai, D. *Proc. Natl. Acad. Sci. U.S.A.* **2007**, *104*, 111–116.

(39) Mu, Y.; Nguyen, P.; Stock, G. *Proteins* **2005**, *58*, 45–52.

(40) Nguyen, P.; Stock, G.; Mittang, G.; Hu, E.; Li, M. *Proteins* **2005**, *61*, 795–808.

(41) Frishman, D.; Argos, P. *Proteins* **1995**, *23*, 566–575.

(42) Garcia, A. *Phys. Rev. Lett.* **1992**, *68*, 2696–2699.

(43) Khandogin, J.; Brooks III, C. *Proc. Natl. Acad. Sci. U.S.A.* **2007**, *104*, 16880–16885.

(44) Yoda, T.; Sugita, Y.; Okamoto, Y. *Chem. Phys. Lett.* **2004**, *386*, 460–467.

(45) Yoda, T.; Sugita, Y.; Okamoto, Y. *Chem. Phys. Lett.* **2004**, *386*, 460–467.

(46) Soto, C.; Castano, E.; Frangione, B.; Inestrosa, N. *J. Biol. Chem.* **1995**, *270*, 3063–3067.

(47) Lazo, N.; Grant, M.; Condron, M.; Rigby, A.; Teplow, D. *Protein Sci.* **2005**, *14*, 1581–1596.

(48) Li, M.; Klimov, D.; Straub, J.; Thirumalai, D. *J. Chem. Phys.* **2008**, *129*, 175101-1–175101-10.

(49) Fawzi, N.; Okabe, Y.; Yap, E.; Gordon, T. *J. Mol. Biol.* **2007**, *365*, 535–550.

(50) Hoyer, W.; Gronwall, C.; Jonsson, A.; Stahl, S.; Hard, T. *Proc. Natl. Acad. Sci. U.S.A.* **2008**, *105*, 5099–5104.

(51) Humphrey, W.; Dalke, A.; Schulten, K. *J. Mol. Graphics* **1996**, *14*, 33–38.

JP808914C